



OPEN

SUBJECT AREAS:

FUEL CELLS

CHEMISTRY

ELECTROCATALYSIS

Received
9 July 2013Accepted
2 September 2013Published
23 September 2013

Correspondence and
requests for materials
should be addressed to
S.H.J. (shjoo@unist.ac.
kr); R.R.A. (adzic@bnl.
gov) or G.-G.P.
(gugon@kier.re.kr)

Ordered mesoporous porphyrinic carbons with very high electrocatalytic activity for the oxygen reduction reaction

Jae Yeong Cheon¹, Taeyoung Kim², YongMan Choi³, Hu Young Jeong^{4,5}, Min Gyu Kim⁶, Young Jin Sa¹, Jaesik Kim¹, Zonghoon Lee⁵, Tae-Hyun Yang², Kyungjung Kwon⁷, Osamu Terasaki^{8,9}, Gu-Gon Park², Radoslav R. Adzic¹⁰ & Sang Hoon Joo¹

¹Department of Chemistry, School of Nano-Bioscience and Chemical Engineering, KIER-UNIST Advanced Center for Energy, and Low-Dimensional Carbon Materials Center, Ulsan National Institute of Science and Technology (UNIST), 50 UNIST-gil, Ulsan 689-798, Republic of Korea, ²Fuel Cell Research Center, Korea Institute of Energy Research (KIER), 152 Gajeongro, Daejeon 305-343, Republic of Korea, ³SABIC Technology Center, Riyadh 11551, Saudi Arabia, ⁴UNIST Central Research Facility, UNIST, 50 UNIST-gil, Ulsan 689-798, Republic of Korea, ⁵School of Mechanical and Advanced Materials Engineering, UNIST, 50 UNIST-gil, Ulsan 689-798, Republic of Korea, ⁶Beamline Research Division, Pohang Accelerator Laboratory (PAL), Pohang 790-784, Republic of Korea, ⁷Department of Energy & Mineral Resources Engineering, Sejong University, Seoul 143-747, Republic of Korea, ⁸Graduate School of EEWS (WCU), Korea Advanced Institute of Science and Technology, 335 Gwahangno, Yuseong-Gu, Daejeon 305-701, Republic of Korea, ⁹Department of Materials and Environmental Chemistry, Berzelii center EXSELENT on Porous Materials, Stockholm University, S-10691, Sweden, ¹⁰Chemistry Department, Brookhaven National Laboratory, Upton, New York 11973-5000, USA.

The high cost of the platinum-based cathode catalysts for the oxygen reduction reaction (ORR) has impeded the widespread application of polymer electrolyte fuel cells. We report on a new family of non-precious metal catalysts based on ordered mesoporous porphyrinic carbons (M-OMPC; M = Fe, Co, or FeCo) with high surface areas and tunable pore structures, which were prepared by nanocasting mesoporous silica templates with metalloporphyrin precursors. The FeCo-OMPC catalyst exhibited an excellent ORR activity in an acidic medium, higher than other non-precious metal catalysts. It showed higher kinetic current at 0.9 V than Pt/C catalysts, as well as superior long-term durability and MeOH-tolerance. Density functional theory calculations in combination with extended X-ray absorption fine structure analysis revealed a weakening of the interaction between oxygen atom and FeCo-OMPC compared to Pt/C. This effect and high surface area of FeCo-OMPC appear responsible for its significantly high ORR activity.

owing to their high energy conversion efficiency and environmental benignity as well as their applicability for small electronic devices, residential power generation, and automobile transportation, polymer electrolyte fuel cells (PEFCs) have long been considered promising energy conversion devices^{1–5}. As electrocatalysts of PEFCs, carbon-supported platinum-based nanoparticles have been used predominantly in anode as well as cathode electrodes^{3–5}. However, even Pt-based electrocatalysts exhibit sluggish kinetics for the oxygen reduction reaction (ORR) at the cathodes of PEFCs. Moreover, they tend to sinter or agglomerate into larger particles during long-term fuel cell operation, resulting in a marked loss of activity⁶. The prohibitively high cost and scarcity of Pt have also been bottlenecks that further impede the widespread use of PEFCs. Therefore, the high cost along with the low durability of Pt-based catalysts triggered the quest for low-cost, high-performance non-precious metal catalysts.

Since Jasinski reported the electrocatalytic activity of Co-phthalocyanine for ORR in an alkaline medium⁷, the class of non-precious metal catalysts has been a topic of continuous interests^{8–36}. The non-precious metal catalysts for ORR consist of naturally abundant transition metals (primarily Fe or Co), nitrogen, and carbon; such catalysts are commonly prepared by mixing the sources of each component, followed by pyrolysis in inert or reactive gas environment^{8–11}. Although synthetic optimization in recent years has led to improved activities and durability of non-precious metal catalysts^{12–23}, particularly in alkali media^{22,23}, their ORR activities are still significantly lower than Pt-based catalysts in acidic electrolytes, as manifested by their larger overpotentials (or half-wave potentials) by 45–400 mV. This situation has required the realistic comparison of the ORR activities of non-precious metal



catalysts at 0.8 V (vs. reversible hydrogen electrode, RHE)³⁷ instead of 0.9 V, at which Pt-based catalysts are commonly gauged³.

Here we report on a simple approach to scalable and highly reproducible synthesis of a new family of non-precious metal catalysts – self-supported, transition metal-doped ordered mesoporous porphyrinic carbons (M-OMPCs) – which exhibit Pt-like catalytic activity for the ORR. The M-OMPC catalysts were prepared by nanocasting ordered mesoporous silica (OMS) templates with metalloporphyrin precursors, and were constructed with three-dimensional networks of porphyrinic carbon frameworks. Our synthetic strategy for the non-precious metal catalysts included a multitude of advantages that would be favourable to PEFC applications. First, our synthetic route is amenable to simple and mild experimental conditions. Previous approaches to non-precious metal-based M-N-C (M = Fe or Co) catalysts relied, in most cases, on the use of two or three separate sources for metal, nitrogen, and carbon^{8–11}. Furthermore, to obtain high ORR activity, employing multiple pyrolysis steps or toxic ammonia gas was unavoidable^{16–20}. In contrast, our method could produce M-N-C catalysts from a single metalloporphyrin precursor in a single pyrolysis step under inert atmosphere without using ammonia gas. Second, the pore size and connectivity of the M-OMPC catalysts were tuneable by utilizing OMS templates with different pore sizes and structures. Third, the synthesis of the M-OMPC catalysts could be readily scaled up, with the preservation of structural integrity, to a few tens of grams in a single batch. Fourth, well-developed, hierarchical micro-mesoporosity would be advantageous for efficient transport of fuels and

by-products. Finally, the M-OMPC catalysts showed very high surface areas, which could significantly increase the density of the catalytically active sites accessible to reactants. Among the family of M-OMPC catalysts, the Fe and Co co-doped OMPC (FeCo-OMPC) showed an extremely high electrocatalytic activity for ORR in acidic media. To our knowledge, its ORR activity is one of the best among the non-precious metal catalysts reported in the literature, and even higher than the state-of-the-art Pt/C catalyst by 80% at 0.9 V (vs. RHE). In addition, the FeCo-OMPC showed superior long-term durability and methanol-tolerance in ORR, compared to the Pt/C. Density functional theory (DFT) calculations coupled with extended X-ray absorption fine structure (EXAFS) analysis revealed a weakening of the interaction between oxygen atom and FeCo-OMPC compared to Pt/C. We attribute the high ORR activity of the FeCo-OMPC to its relatively weak interaction with oxygen as well as the high surface area design of catalyst.

Results

Synthesis and structural characterization of M-OMPC catalysts.

Figure 1a schematically shows our synthetic strategy based on a nanocasting method for the preparation of the M-OMPC catalysts using OMSs as hard templates [see details in the Supplementary Information]. The nanocasting method has proven to be very effective for generating nanoporous carbon structures^{38–41}. As representative examples, 1 g of a metalloporphyrin precursor was mixed with 1 g of the SBA-15 template (Supplementary Fig. S1), and the mixture was pyrolysed at 800 °C under nitrogen. The use

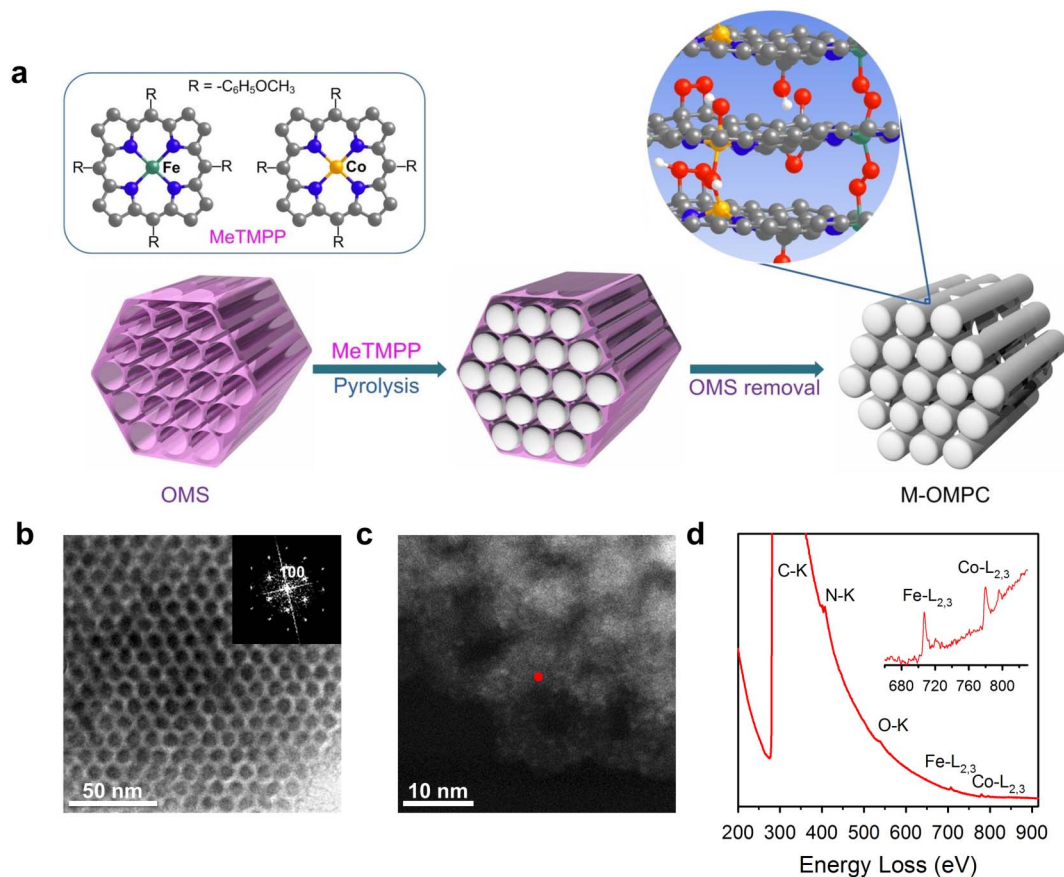


Figure 1 | Synthetic strategy and characterisation of M-OMPC catalysts. (a) Schematic synthetic strategy. The M-OMPC catalysts were synthesized via a nanocasting method that employed OMSs as templates and metalloporphyrins as the carbon source. The high temperature pyrolysis resulted in an OMS/carbon composite, after which the final M-OMPC catalysts were generated through the removal of the OMS template by HF etching. Grey, blue, green, orange, red, and white spheres represent C, N, Fe, Co, O, and H, respectively. (b) TEM image and the corresponding Fourier diffractogram (inset) of FeCo-OMPC templated from SBA-15 mesoporous silica showing hexagonal arrays of uniform carbon nanorods and mesopores generated between the nanorods. (c) HAADF STEM image of FeCo-OMPC catalyst. (d) EELS at the region of the red spot in the HAADF STEM image.



of 5,10,15,20-tetrakis(4-methoxyphenyl)-21H,23H-porphine iron(III) chloride (FeTMPPCl), 5,10,15,20-tetrakis(4-methoxyphenyl)-21H, 23H-porphine cobalt(II) (CoTMPP), or a 1:1 (mass ratio) mixture of FeTMPPCl and CoTMPP as precursors afforded Fe-OMPC, Co-OMPC, or FeCo-OMPC, respectively. The transmission electron microscopy (TEM) image of the FeCo-OMPC (Fig. 1b) clearly showed that uniform carbon nanorods of 10 nm in diameter were arranged in a honeycomb-like hexagonal structure, with uniform mesopores being generated between the carbon nanorods. This clearly indicates that the SBA-15 silica template was faithfully replicated into a negative replica, FeCo-OMPC. Interestingly, the TEM image of the FeCo-OMPC before the etching of the SBA-15 template (Supplementary Fig. S2) contained crystalline FeCo particles 10–20 nm in diameter. We suppose that during high-temperature pyrolysis, the Fe and Co atoms in the metalloporphyrin precursors were progressively converted to metallic nanoparticles, with the latter being almost removed during the HF washing step. The TEM images of the final FeCo-OMPC sample indicated no formation of metallic particles, although the possible existence of very small metallic particles (< 1 nm) cannot be ruled out. The low-angle X-ray diffraction patterns of M-OMPCs (Supplementary Fig. S3) exhibited three distinct diffraction lines corresponding to the (100), (110), and (200) planes of the hexagonal mesostructure. The nitrogen adsorption analysis of the FeCo-OMPC (Supplementary Fig. S4a) revealed that the catalyst had well-developed mesoporosity and high surface areas. The pore size distribution curve of the FeCo-OMPC (Supplementary Fig. S4b) analysed by the Barrett-Joyner-Halenda and the Horvath-Kawazoe methods showed peak maxima at 4.9 nm (mesopore) and 0.5 nm (micropore), respectively. The high porosity of FeCo-OMPC stemming from the hierarchical micro-mesopores provided a very high Brunauer-Emmett-Teller (BET) surface area of 1,190 m² g⁻¹ and a total pore volume of 1.40 cm³ g⁻¹ (Supplementary Table S1). The nanocasting employing metalloporphyrin precursors is general, and could be extended to other OMS templates; the nanocasting using MSU-F silica with large, spherical mesopores and KIT-6 with cubic *Ia3d* mesostructure yielded large pore (ca. 20 nm) FeCo-OMPC(L) (Supplementary Fig. S5 and Table S1) and FeCo-OMPC(C) with gyroid mesostructure (Supplementary Fig. S6 and Table S1), respectively.

We analysed the distribution and chemical states of the elements in the FeCo-OMPC. The high angle annular dark field scanning transmission electron microscopy (HAADF STEM) image (Fig. 1c) showed bright dots corresponding to heavy elements (Fe and Co), which were uniformly distributed over a single particle. Furthermore, an electron energy loss spectroscopy (EELS) spectrum (Fig. 1d) acquired at the red spot in Figure 1c clearly indicated the presence of C, N, O, Fe, and Co. The X-ray photoelectron spectroscopy (XPS) survey spectrum of the FeCo-OMPC (Supplementary Fig. S7a) also revealed the presence of C, N, O, Fe, and Co on the surface of the catalyst. The detailed analysis of the N 1s spectrum (Supplementary Fig. S7b) showed three peaks centred at 398.2, 399.8, and 401.8 eV, which could be associated with pyridinic, pyrrolic or metal-N, and graphitic groups, respectively. Inductively coupled plasma–optical emission spectroscopy analysis and CHNS elemental analysis indicated that the amounts of Fe, Co, and N in the FeCo-OMPC pyrolysed at 800 °C were 2.5, 2.3, and 5.4 wt%, respectively.

ORR activity and durability of M-OMPC catalysts. We next explored the electrocatalytic activity of the M-OMPC catalysts along with reference catalysts using rotating ring-disk electrode (RRDE) measurements in 0.1 M HClO₄ solution (Fig. 2). In general, M-OMPC catalysts showed very high ORR activity, compared to other catalysts. Of the various M-OMPC catalysts, FeCo-OMPC pyrolysed at 800 °C under N₂ showed the highest ORR activity. FeCo-OMPC showed on-set and half-wave potentials at 1.000 V and 0.851 V, respectively (Fig. 2a), and its kinetic current density

at 0.9 V, calculated after correction for diffusion-limited current, was 2.42 mA cm⁻² (Fig. 2b). Significantly, such a high ORR activity of the FeCo-OMPC catalyst was remarkably reproducible, which was verified by very low standard deviations of kinetic data obtained with 30 sample batches of FeCo-OMPC (Supplementary Table S2). The other M-OMPC catalysts also showed very high electrocatalytic activities for ORR. The large pore FeCo-OMPC(L) and monometal-doped Fe-OMPC and Co-OMPC catalysts exhibited ORR polarisation curves similar to that of FeCo-OMPC, with their half-wave potentials being shifted to lower potentials by only less than 45 mV, compared to that of the FeCo-OMPC (Fig. 2a). We note that the synergistic effect of two different metal centres (Fe and Co) in enhancing ORR activity was also observed in previous studies^{20,25,32}.

The very high ORR activity of FeCo-OMPC catalyst for the ORR was remarkable, and a comparison with previously reported catalysts indicates FeCo-OMPC as one of the best non-precious metal ORR catalysts (Supplementary Table S3), along with the recent result from Dodelet and co-workers¹⁸. The half-wave potential of the FeCo-OMPC was significantly shifted to positive potentials by 50 to 100 mV, compared to those of previously reported non-precious metal catalysts. Particularly, comparing the kinetic current density at 0.9 V, the FeCo-OMPC showed significant current density (2.42 mA cm⁻²) whereas the previous catalysts exhibited only negligible currents for ORR at this potential. Further comparison at 0.8 V where non-precious metal catalysts are commonly compared revealed that the kinetic current density of the FeCo-OMPC was up to 30 times higher than the other catalysts (Supplementary Table S3).

We also compared the ORR activities of M-OMPCs with the reference catalysts. To identify the role of the metal atom (Fe or Co), we prepared a metal-free OMPC from 5,10,15,20-tetrakis(4-methoxyphenyl)-21H,23H porphyrin (TMPPH) precursor (Supplementary Fig. S8 and Table S1). The metal-free OMPC showed electrocatalytic current for ORR, but its on-set and half-wave potentials were markedly shifted to lower potentials, compared to those of the M-OMPC catalysts (Fig. 2a), suggesting a crucial role of metal atoms in catalysing oxygen reduction. Next, we measured the ORR activity of two metalloporphyrin-driven catalysts. The first sample was prepared by impregnating a mixed precursor of FeTMPPCl and CoTMPP onto a carbon black (Ketjenblack®, KB) support, followed by pyrolysis at 800 °C (Supplementary Table S1)²⁷. The ORR activity of the resulting FeCo-KB catalyst was significantly lower than the M-OMPC catalysts, as manifested by markedly lower on-set and half-wave potentials (Fig. 2a). The other metalloporphyrin-driven catalyst was prepared by a nanocasting method using amorphous silica particles (Cab-O-Sil®, Cabosil) as a template and a mixture of FeTMPPCl and CoTMPP as a precursor, following the previous reports (Supplementary Fig. S9 and Table S1)^{25,29,30}. Thus prepared FeCo-Cabosil catalyst showed better ORR activity than the FeCo-KB catalyst, yet its on-set and half-wave potentials were negatively shifted by 100 mV, compared to FeCo-OMPC catalyst, indicating much inferior ORR activity. The ORR activity of these reference catalysts indicates that the important role of metal in catalysing ORR as well as high surface area and mesostructure of carbon support in enhancing ORR activity.

To assess the pathway of ORR over the M-OMPC catalysts, we measured ring currents, from which the number of electrons transferred during ORR was calculated. Figure 2c shows that the number of transferred electrons was above 3.9 over all potentials by the FeCo-OMPC catalyst, and the number approached 4 at a potential near 0.9 V. This clearly indicates that ORR catalysed by the FeCo-OMPC followed a 4-electron pathway, which is typically shown by the Pt/C catalyst³.

We further compared the ORR activity of the FeCo-OMPC with the Pt/C (20 wt% Pt supported on Vulcan carbon, E-TEK) catalyst. We found that the very high activity of the FeCo-OMPC was even

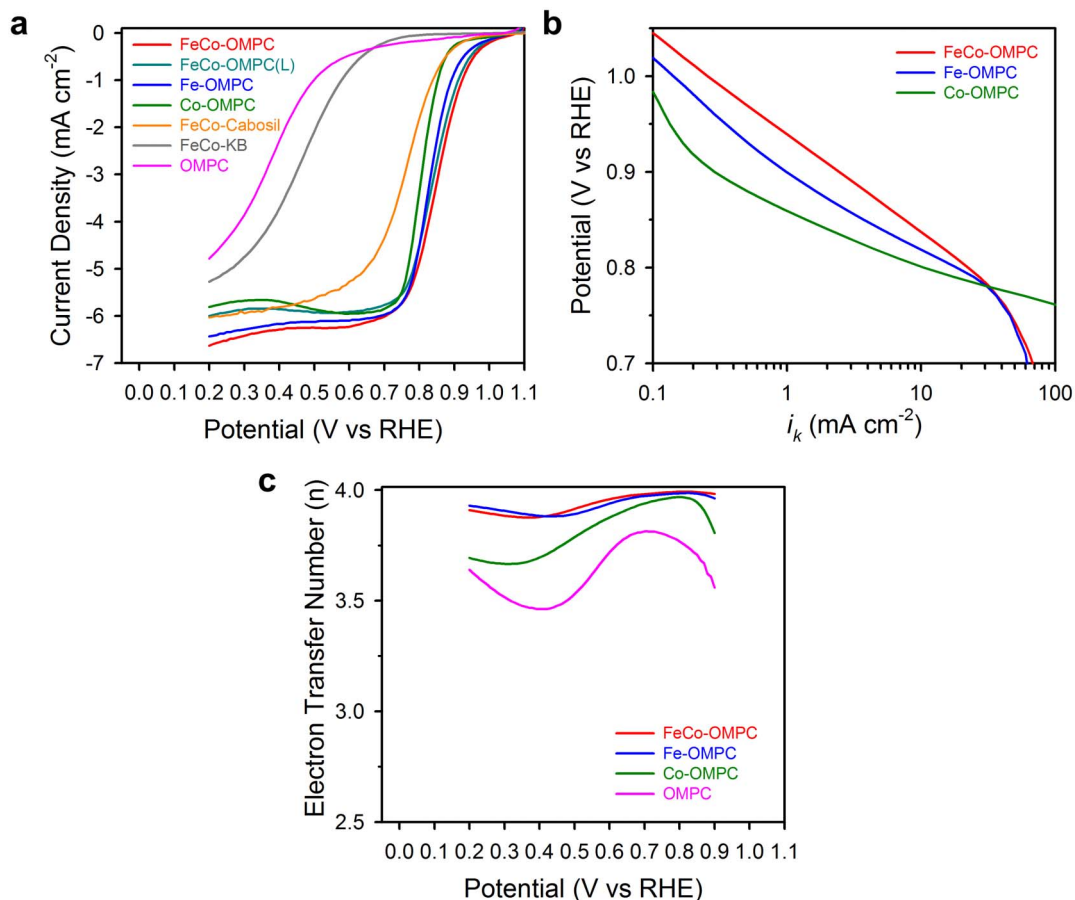


Figure 2 | ORR activity of M-OMPC catalysts. (a) ORR polarisation curves of M-OMPC (M=FeCo, Fe, Co), FeCo-OMPC(L), OMPC, and FeCo-KB catalysts in O_2 -saturated 0.1 M $HClO_4$. (b) Tafel plots derived from the corresponding ORR polarisation curves after mass transport correction. (c) Number of electrons transferred during ORR calculated based on ring currents. For all RRDE measurements, the catalyst loadings were 0.6 mg cm^{-2} . The electrode rotation speed was 1600 rpm and the scan rate was 5 mV s^{-1} .

better than the Pt/C catalyst (Fig. 3a,b and Supplementary Fig. S10, Table S4). The ORR activity measured with a very slow scan rate of 1 mV s^{-1} , under which the contribution from the capacitive current could be virtually excluded, higher ORR activity for the FeCo-OMPC catalyst over Pt/C was clearly observed (Fig. 3a). Importantly, the kinetic current density of the FeCo-OMPC at 0.9 V (1.80 mA cm^{-2}) surpassed that of the Pt/C catalyst (1.00 mA cm^{-2}) by 80% (Fig. 3b and Supplementary Table S4). The half-wave potentials of the two catalysts were 0.845 V and 0.840 V for the FeCo-OMPC and Pt/C, respectively. The FeCo-OMPC catalyst also showed very high electrocatalytic activity in an alkaline medium. The ORR polarisation curve of the FeCo-OMPC catalyst in 0.1 M KOH was nearly identical to that of the Pt/C catalyst (Supplementary Fig. S11).

For the sustainable use of fuel cell electrocatalysts, their long-term durability is critical. We explored the durability of the FeCo-OMPC catalyst by cycling the catalysts 10,000 times between 0.6 and 1.0 V (vs. RHE) at a scan rate of 50 mV s^{-1} , following the accelerated durability test protocol of the U.S. Department of Energy (DOE)³⁷. The changes in half-wave potentials as well as kinetic current densities between the cycling tests indicated that the FeCo-OMPC catalyst exhibited superior durability over the Pt/C catalyst. After cycling 10,000 times with N_2 bubbling the FeCo-OMPC catalyst underwent a negative shift of 24 mV in half-wave potential, whereas the Pt/C catalyst showed a negative shift of 45 mV (Supplementary Fig. S12). Under O_2 bubbling conditions, negative shifts of 30 and 65 mV in the half-wave potentials were observed for the FeCo-OMPC and the Pt/C catalysts, respectively (Fig. 3c and Supplementary Fig. S13). Before the cycling tests, the FeCo-OMPC showed a kinetic current

density of 2.44 mA cm^{-2} at 0.9 V, which was higher than the Pt/C catalyst (1.76 mA cm^{-2}) by 39% (Fig. 3d). After cycling 10,000 times under O_2 , the performance gap between the two catalysts increased even further: FeCo-OMPC (1.31 mA cm^{-2}) exhibited an almost six-fold higher ORR activity than Pt/C (0.23 mA cm^{-2}) (Fig. 3d). The better durability of the FeCo-OMPC catalyst may stem from its higher tolerance to the agglomeration of metallic species. We next addressed the tolerance of the FeCo-OMPC catalyst against poisoning with fuel molecules, which is directly relevant to its potential use in direct alcohol fuel cells. The ORR polarisation curve of the FeCo-OMPC in the presence of 0.5 M methanol (Supplementary Fig. S14) exhibited only a small shift of half-wave potential (30 mV). In contrast, the Pt/C catalyst showed a significant negative shift (305 mV) owing to the poisoning of the surfaces of the Pt nanoparticles by CO, the decomposition product of $MeOH$ ^{21,42}.

Discussion

In order to analyse the structure of highly active catalysts for ORR, we investigated the local structure of the FeCo-OMPC catalyst with EXAFS and X-ray absorption near edge structure (XANES) analysis. The comparison of XANES spectra (Supplementary Fig. S15) revealed that the square-planar D_{4h} local symmetry shown by model compounds (Fe-phthalocyanine for Fe, and CoTMPP for Co) was broken down in the FeCo-OMPC catalyst, possibly due to the additional coordination along the axial direction. The radial distribution functions (RDFs) for the Fe (Fig. 4a) and Co (Fig. 4b) K-edge EXAFS spectra provided more detailed evidence for the breakdown of the square-planar symmetry in the FeCo-OMPC catalyst. The RDF of Fe

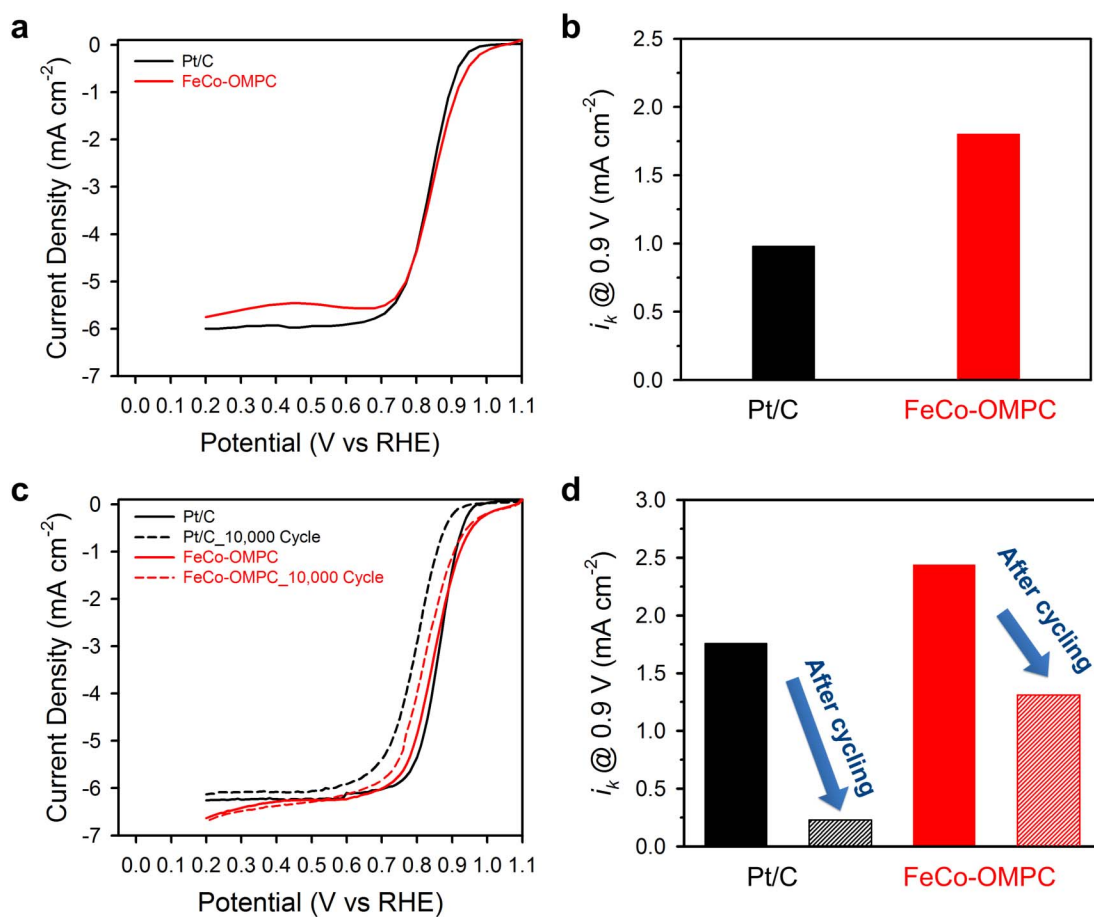


Figure 3 | Comparison of activity and durability of Pt/C and FeCo-OMPC. (a) ORR polarisation curves of Pt/C and FeCo-OMPC catalysts in O₂-saturated 0.1 M HClO₄ at the scan rate of 1 mV s⁻¹. (b) Corresponding kinetic currents of Pt/C and FeCo-OMPC catalysts at the scan rate of 1 mV s⁻¹. (c) ORR polarisation curves of Pt/C and FeCo-OMPC catalysts before and after 10,000 potential cycles in O₂-saturated 0.1 M HClO₄. Potential cycling was carried out from 0.6 to 1.0 V vs. RHE at 50 mV s⁻¹. (d) Comparison of kinetic currents of Pt/C and FeCo-OMPC catalysts before and after 10,000 potential cycles. For all RRDE measurements, the catalyst loadings were 0.6 mg cm⁻² for FeCo-OMPC catalyst and 20 μg_{Pt} cm⁻² for Pt/C. The electrode rotation speed was 1,600 rpm and the scan rate was 5 mV s⁻¹.

K-edge of the FeCo-OMPC catalyst showed two newly evolved FT peak features, compared to model compounds, that could be assigned to an additional oxygen molecule coordinated in the axial direction on the central Fe atom, with a shorter O₁ and longer O₂, respectively. On the other hand, the RDF of Co K-edge showed a single axial-coordination by the oxygen atom (OH). It is noteworthy that the distinct FT peak at around 4.3 Å at the Fe K-edge RDF corresponded to the chemical bonding interaction of Fe-(O₂)-Fe by way of the oxygen molecule as a pillaring element between the interlayers, which is similar to the structure of face-to-face porphyrin-based ORR catalyst⁴³. Based on the EXAFS curve-fitting results, structural parameters around each metal, including bond distances and coordination numbers were obtained and summarized in Table S5.

We then constructed several models (Supplementary Fig. S16) for DFT calculations based on the experimental findings. On the basis of the EXAFS data, DFT calculations using bilayer **Model III** suggested that the Co centres were connected with OH (~ 0.98 Å), while the Fe centres were connected with OO (~ 1.40 Å) (Fig. 4c). We found that the averaged M-M distance of the 2-layer model (**Model III**) was ~ 4.6 Å, which was in good agreement with the EXAFS results as well as the HRTEM observation of interlayer distances (4.8 Å) within the FeCo-OMPC frameworks (Supplementary Fig. S17). We carried out DFT calculations to elucidate the enhanced ORR activity of the FeCo-OMPC catalyst compared to those of Fe-OMPC, Co-OMPC,

and Pt/C catalysts. We adopted the binding energy of atomic oxygen (BO) as a descriptor for calculating ORR activities⁴⁴. Two oxygen atoms were placed at the active metal sites on the surface [see Supplementary Information for details]. First, we used a small bilayer (0001) surface generated from **Model IV** bulk structure. The change of the metal centres and bridging species from the mixed FeCo-OMPC to pure Fe- or Co-OMPC led to strengthened O-surface interactions (-3.14 eV/atom for FeCo-OMPC and -4.94 eV/atom and -4.02 eV/atom for Fe-OMPC and Co-OMPC, respectively) (Supplementary Fig. S18 and Table S6). Furthermore, we found that Fe more strongly binds O than Co on FeCo-OMPC (-3.52 eV versus -2.79 eV, respectively). This indicates that a proper mixing of Fe and Co decreased the binding energy of oxygen. It is well known that a slight weakening of the O interaction with catalyst surfaces is a key factor in down-shifting of the d-band centres, thereby increasing the ORR activity⁴⁵. In a further comparison with Pt(111) using a more realistic **Model II** surface (Fig. 4d), the FeCo-OMPC catalyst (-3.33 eV/atom) showed a slight decrease in BO from that of Pt(111) (-3.58 eV/atom), indicating an enhanced ORR activity of the FeCo-OMPC catalyst over Pt(111).

Based on the results from various characterization methods and the DFT calculation, the very high activity of M-OMPC catalysts, particularly FeCo-OMPC, appears to originate from a combination of several factors. The nanocasting from OMS templates afforded ordered mesoporous catalysts with very high surface area, wherein

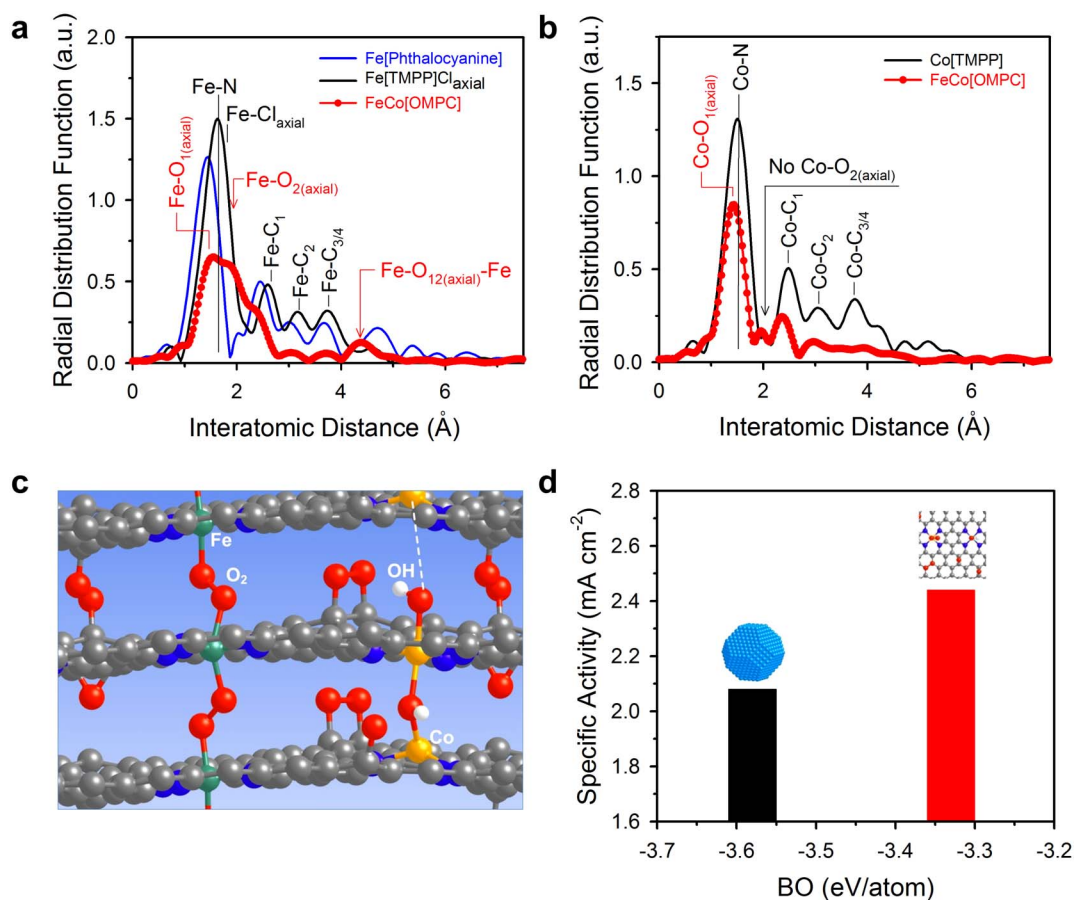


Figure 4 | EXAFS and DFT results. (a, b) Radial distribution functions of Fourier-transformed k^2 -weighted Fe (a) and Co (b) K-edge EXAFS for FeCo-OMPC catalyst, in comparison with reference materials. (c) Schematic of a representative FeCo-OMPC model. Grey, blue, green, orange, red, and white spheres represent C, N, Fe, Co, O, and H, respectively. (d) DFT results of specific activity against binding energy of atomic oxygen (BO) over Pt/C and FeCo-OMPC catalysts.

the number of porphyrinic active sites could be enlarged. The direct conversion of porphyrin precursor inside the nanopores of the OMS template allowed for catalytically active M-N bondings intact in the final carbogenic structures, as proved by EXAFS. In addition, the combined use of two different metal centres (Fe and Co) could endow synergistic effect in FeCo-OMPC, which was manifested as weakened interaction with oxygen, compared to monometal-doped OMPCs and Pt(111) surface.

We carried out preliminary single cell tests for a PEFC that employed the large pore FeCo-OMPC(L) as a cathode catalyst. The open circuit voltage of single cell was 0.98 V under pure oxygen condition. The current density and power density of the single cell at 0.6 V were 513 mA cm⁻² and 0.308 W cm⁻², respectively (Fig. 5a). The volumetric activity at 0.8 V (Fig. 5b), obtained from the intersection of the extrapolated Tafel slope (dashed line) with the 0.8 V axis, was 131 A cm⁻³ (solid red circle), which showed a high

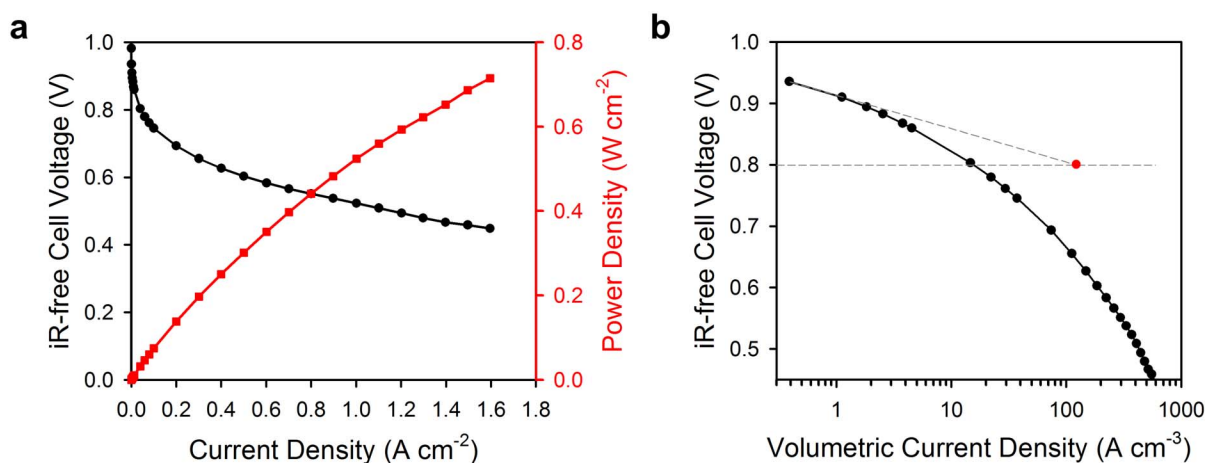


Figure 5 | PEFC single cell performance. (a) iR-corrected polarisation plot of H₂-O₂ fuel cell employing FeCo-OMPC(L) as a cathode catalyst (the red line is the corresponding power density). (b) Volumetric current density vs. iR-free cell voltage.



possibility of achieving the US DOE's target of FY 2017³⁷. We also performed long-term durability test using FeCo-OMPC(L) catalyst as a cathode (Supplementary Fig. S19). At an operating voltage of 0.5 V, the single cell showed an initial current density of 0.5 A cm⁻². The single cell underwent a drop in current density until 40 h under operation, yet after which it showed steady current density at 0.2 A cm⁻². These PEFC single cell results need improvement in terms of both activity and durability.

In summary, we have presented a new family of electrocatalysts based on the ordered mesoporous porphyrinic architecture, which showed a very high ORR activity in an acidic medium that compares favourably to Pt/C catalysts. We attribute the high activity of the FeCo-OMPC catalyst to its weak interaction with oxygen, its high surface area that can expose a high density of active sites, and the use of porphyrin precursors. The M-OMPC catalysts also showed enhanced durability and poison-tolerance, compared to the Pt/C catalysts. Significantly, we point out that the synthetic route to M-OMPC catalysts is very simple and general and is amenable to large scale synthesis. Recent years have witnessed a rapid progress in the development of electrocatalysts for ORR. For instance, nanoparticles composed of a Pt monolayer on PdAu core⁴⁶, intermetallic Pt-Co nanoparticles⁴⁷, and mesostructured PtNi thin films⁴⁸ have demonstrated significantly improved ORR activity and durability in acidic media. We believe that, along with these new catalysts, the M-OMPCs could emerge as highly promising ORR catalysts. Furthermore, the design concept towards enhanced electrocatalytic performances presented in this work could be extended to other electrocatalytic reactions in energy devices, such as metal-air batteries and electrolyzers.

Methods

Synthesis of catalysts. Synthesis of catalysts M-OMPC catalysts were synthesized by a solid-state nanocasting method^{49,50} that used OMS as a template and FeTMPPCl (Porphyrin Systems) and CoTMPP (TCI) as precursors. Calcined OMS (1.0 g) was mixed with the precursor (1.0 g), and the mixture was ground for 10 min in a mortar and transferred to an alumina crucible. The mixture was subsequently heated at temperatures ranging from 600 °C to 1000 °C with a ramping rate of 2.5 °C min⁻¹, and was held at a specific temperature for 3 h under nitrogen flow. The resulting carbon-silica composite was then washed twice with 10% HF (J. T. Baker) at room temperature for 1 h to remove the OMS template.

Electrochemical characterisation. The electrochemical characterization of the catalysts was performed using an IviumStat electrochemical analyser. The characterization experiments were performed at room temperature (25 °C) using a three-electrode electrochemical cell. A Pt-wire counter electrode separated by fritted glass and an Ag/AgCl reference electrode were used. All potentials in this study were reported with respect to the RHE. A rotating ring-disk electrode (RRDE) was used as a working electrode. The RRDE was polished with a 1.0 μm alumina suspension and then with a 0.3 μm suspension to afford a mirror finish. The catalyst (30 mg) was mixed with deionized (DI) water (0.1 mL), ethanol (1.01 mL), and Nafion® (0.075 mL, 5 wt% in isopropanol, Aldrich). The resulting slurry was ultra-sonicated for 30 min to generate a catalyst ink. The ink (3.0 μL) was pipetted onto the 0.126 cm² glassy carbon electrode, resulting in a catalyst loading of 596 μg cm⁻². Before the electrochemical measurements, the catalyst was cleaned by cycling the potential between 0 and 1.2 V at 100 mV s⁻¹ for 50 cycles using a N₂-saturated 0.1 M HClO₄ solution as an electrolyte. Cyclic voltammetry (CV) was performed over voltages ranging from 0 to 1.2 V at a scan rate of 20 mV s⁻¹ using a N₂-saturated 0.1 M HClO₄ electrolyte. ORR activity was recorded in O₂-saturated 0.1 M HClO₄ electrolyte with linear sweep voltammetry (LSV) performed for voltages ranging from 1.1 to 0.2 V at a scan rate of 5 mV s⁻¹. The disk rotation speed was 100–2500 rpm. Commercial 20 wt% platinum on Vulcan® carbon black (Pt/C, E-TEK) was measured for comparison. The catalyst ink was prepared as follows. The Pt/C catalyst (5 mg) was mixed with DI water (0.1 mL), ethanol (1.07 mL), and Nafion® (0.013 mL). Other experimental conditions were the same as for the M-OMPC catalysts, except that ORR activity data were collected from anodic sweeps. The durability tests were performed on the catalysts by cycling the electrode potential between 0.6 and 1.0 V at 50 mV s⁻¹ for 10,000 cycles.

- Steele, B. C. H. & Heinzel, A. Materials for fuel-cell technologies. *Nature* **414**, 345–352 (2001).
- Arico, A. S., Bruce, P., Scrosati, B., Tarascon, J.-M. & Van Schalkwijk, W. Nanostructured materials for advanced energy conversion and storage devices. *Nat. Mater.* **4**, 366–377 (2005).
- Gasteiger, H. A., Kocha, S. S., Sompalli, B. & Wagner, F. T. Activity benchmarks and requirements for Pt, Pt-alloy, and non-Pt oxygen reduction catalysts for PEMFCs. *Appl. Catal. B* **56**, 9–35 (2005).
- Debe, M. K. Electrocatalyst approaches and challenges for automotive fuel cells. *Nature* **486**, 43–51 (2012).
- Rabis, A., Rodriguez, P. & Schmidt, T. J. Electrocatalysis for polymer electrolyte fuel cells: Recent achievements and future challenges. *ACS Catal.* **2**, 864–890 (2012).
- Borup, R. *et al.* Scientific aspects of polymer electrolyte fuel cell durability and degradation. *Chem. Rev.* **107**, 3904–3951 (2007).
- Jasinski, R. A new fuel cell cathode catalyst. *Nature* **201**, 1212–1213 (1964).
- Wang, B. Recent development of non-platinum catalysts for oxygen reduction reaction. *J. Power Sources* **152**, 1–15 (2005).
- Bezerra, C. W. B. *et al.* A review of Fe-N/C and Co-N/C catalysts for the oxygen reduction reaction. *Electrochim. Acta* **53**, 4937–4951 (2008).
- Jaouen, F. *et al.* Recent advances in non-precious metal catalysis for oxygen-reduction reaction in polymer electrolyte fuel cells. *Energy Environ. Sci.* **4**, 114–130 (2011).
- Chen, Z., Higgins, D., Yu, A., Zhang, L. & Zhang, J. A review on non-precious metal electrocatalysts for PEM fuel cells. *Energy Environ. Sci.* **4**, 3167–3192 (2011).
- Gupta, S., Tryk, D., Bae, I., Aldred, W. & Yeager, E. Heat-treated polyacrylonitrile-based catalysts for oxygen electroreduction. *J. Appl. Electrochem.* **19**, 19–27 (1989).
- Lefevre, M., Dodelet, J.-P. & Bertrand, P. Molecular oxygen reduction in PEM fuel cells: Evidence for the simultaneous presence of two active sites in Fe-based catalysts. *J. Phys. Chem. B* **106**, 8705–8713 (2002).
- Jaouen, F., Lefevre, M., Dodelet, J.-P. & Cai, M. Heat-treated Fe/N/C catalysts for O₂ electroreduction: Are active sites hosted in micropores? *J. Phys. Chem. B* **110**, 5553–5558 (2006).
- Bashyam, R. & Zelenay, P. A class of non-precious metal composite catalysts for fuel cells. *Nature* **443**, 63–66 (2006).
- Lefevre, M., Proietti, E., Jaouen, F. & Dodelet, J.-P. Iron-based catalysts with improved oxygen reduction activity in polymer electrolyte fuel cells. *Science* **324**, 71–74 (2009).
- Proietti, E. *et al.* Iron-based cathode catalyst with enhanced power density in polymer electrolyte membrane fuel cells. *Nat. Commun.* **2**, 416 (2011).
- Jaouen, F. *et al.* Oxygen reduction activities compared in rotating-disk electrode and proton exchange membrane fuel cells for highly active Fe-N-C catalysts. *Electrochim. Acta* **87**, 619–628 (2013).
- Wu, L. *et al.* Pt-free cathode catalysts prepared via multi-step pyrolysis of Fe phthalocyanine and phenolic resin for fuel cells. *Chem. Commun.* **46**, 6377–6379 (2010).
- Wu, G., More, K. L., Johnston, C. M. & Zelenay, P. High-performance electrocatalysts for oxygen reduction derived from polyaniline, iron, and cobalt. *Science* **332**, 443–447 (2011).
- Li, Y. *et al.* An oxygen reduction electrocatalyst based on carbon nanotube-graphene complexes. *Nat. Nanotech.* **7**, 394–400 (2012).
- Chung, H. T., Won, J. H. & Zelenay, P. Active and stable carbon nanotube/nanoparticle composite electrocatalyst for oxygen reduction. *Nat. Commun.* **4**, 1922 (2013).
- Li, Y. *et al.* Advanced zinc-air batteries based on high-performance hybrid electrocatalysts. *Nat. Commun.* **4**, 1805 (2013).
- Kosłowski, U. I., Abs-Wurmbach, I., Fiechter, S. & Bogdanoff, P. Nature of the catalytic centers of porphyrin-based electrocatalysts for the ORR: A correlation of kinetic current density with the site density of Fe-N₄ centers. *J. Phys. Chem. C* **112**, 15356–15366 (2008).
- Nallathambi, V., Lee, J.-W., Kumaraguru, S. P., Wu, G. & Popov, B. N. Development of high performance carbon composite catalyst for oxygen reduction reaction in PEM proton exchange membrane fuel cells. *J. Power Sources* **183**, 34–42 (2008).
- Garsuch, A. *et al.* Oxygen reduction behavior of highly porous non-noble metal catalysts prepared by a template-assisted synthesis route. *J. Electrochem. Soc.* **155**, B236–B243 (2008).
- Charreter, F., Jaouen, F. & Dodelet, J.-P. Iron porphyrin-based cathode catalysts for PEM fuel cells: Influence of pyrolysis gas on activity and stability. *Electrochim. Acta* **54**, 6622–6630 (2009).
- Jaouen, F. *et al.* Cross-laboratory experimental study of non-noble-metal electrocatalysts for the oxygen reduction reaction. *ACS Appl. Mater. Interfaces* **1**, 1623–1639 (2009).
- Olson, T. S., Pylypenko, S., Fulghum, J. E. & Atanassov, P. Bifunctional oxygen reduction reaction mechanism on non-platinum catalysts derived from pyrolyzed porphyrins. *J. Electrochem. Soc.* **157**, B54–B63 (2010).
- Choi, J.-Y., Hsu, R. S. & Chen, Z. Highly active porous carbon-supported nonprecious metal-N electrocatalyst for oxygen reduction reaction in PEM fuel cells. *J. Phys. Chem. C* **114**, 8048–8053 (2010).
- Wu, G. *et al.* Synthesis-structure-performance correlation for polyaniline-Me-C non-precious metal cathode catalysts for oxygen reduction in fuel cells. *J. Mater. Chem.* **21**, 11392–11405 (2011).
- Wu, G. *et al.* Synthesis of nitrogen-doped onion-like carbon and its use in carbon-based CoFe binary non-precious-metal catalysts for oxygen-reduction. *Carbon* **49**, 3972–3982 (2011).



33. Ma, S., Goenaga, G. A., Call, A. V. & Liu, D.-J. Cobalt imidazolate framework as precursor for oxygen reduction reaction electrocatalysts. *Chem-Eur. J.* **17**, 2063–2067 (2011).
34. Lee, D. H., Lee, W. J., Kim, S. O. & Kim, Y.-H. Theory, synthesis, and oxygen reduction catalysis of Fe-porphyrin-like carbon nanotube. *Phys. Rev. Lett.* **106**, 175502 (2011).
35. Byon, H. R., Suntivich, J. & Shao-Horn, Y. Graphene-based non-noble-metal catalysts for oxygen reduction reaction in acid. *Chem. Mater.* **23**, 3421–3428 (2011).
36. Dombrovskis, J. K., Jeong, H. Y., Fossum, K., Terasaki, O. & Palmqvist, A. E. C. Transition metal ion-chelating ordered mesoporous carbons as noble metal-free fuel cell catalysts. *Chem. Mater.* **25**, 856–861 (2013).
37. *The US DRIVE Fuel Cell Technical Team Technology Roadmap (Revised August 11, 2011)* <http://www.uscar.org/guest/tlc/2/Hydrogen-Fuel-Cell-TLC>. Accessible: September 18, 2012.
38. Lu, A.-H. & Schüth, F. Nanocasting: A versatile strategy for creating nanostructured porous materials. *Adv. Mater.* **18**, 1793–1805 (2006).
39. Joo, S. H. *et al.* Ordered nanoporous arrays of carbon supporting high dispersions of platinum nanoparticles. *Nature* **412**, 169–172 (2001).
40. Ma, Z., Kyotani, T. & Tomita, A. Preparation of a high surface area microporous carbon having the structural regularity of Y zeolite. *Chem. Commun.* 2365–2366 (2000).
41. Liu, B., Shioyama, H., Akita, T. & Xu, Q. Metal-organic framework as a template for porous carbon synthesis. *J. Am. Chem. Soc.* **130**, 5390–5391 (2008).
42. Kwon, K., Sa, Y. J., Cheon, J. Y. & Joo, S. H. Ordered mesoporous carbon nitrides with graphitic frameworks as metal-free, highly durable, methanol-tolerant oxygen reduction catalysts in an acidic medium. *Langmuir* **28**, 991–996 (2012).
43. Collman, J. P. *et al.* Electrode catalysis of the four-electron reduction of oxygen to water by dicobalt face-to-face porphyrins. *J. Am. Chem. Soc.* **102**, 6027–6036 (1980).
44. Greeley, J. *et al.* Alloys of platinum and early transition metals as oxygen reduction electrocatalysts. *Nat. Chem.* **1**, 552–556 (2009).
45. Zhang, J. L. *et al.* Controlling the catalytic activity of platinum monolayer electrocatalysts for oxygen reduction with different substrates. *Angew. Chem., Int. Ed.* **44**, 2132–2135 (2005).
46. Sasaki, K. *et al.* Highly stable Pt monolayer on PdAu nanoparticle electrocatalysts for the oxygen reduction reaction. *Nat. Commun.* **3**, 1115 (2012).
47. Wang, D. *et al.* Structurally ordered intermetallic platinum–cobalt core–shell nanoparticles with enhanced activity and stability as oxygen reduction electrocatalysts. *Nat. Mater.* **12**, 81–87 (2013).
48. van der Vliet, D. F. *et al.* Mesostructured thin films as electrocatalysts with tunable composition and surface morphology. *Nat. Mater.* **11**, 1051–1058 (2012).
49. Lee, K. T., Ji, X., Rault, M. & Nazar, L. F. Simple synthesis of graphitic ordered mesoporous carbon materials by a solid-state method using metal phthalocyanines. *Angew. Chem., Int. Ed.* **48**, 5661–5665 (2009).
50. Jo, Y. *et al.* Highly interconnected ordered mesoporous carbon – carbon nanotube nanocomposites: Pt-free, highly efficient, and durable counter electrode for dye-sensitized solar cells. *Chem. Commun.* **48**, 8057–8059 (2012).

Acknowledgements

S.H.J. was supported by the Basic Science Research Program through the National Research Foundation (NRF) of Korea, funded by the Ministry of Education (NRF-2013R1A1A2012960) and the TJ Park Junior Faculty Fellowship. G.-G.P. acknowledges the support from Korea Institute of Energy Research (KIER, B3-2415). R.R.A. was supported by U.S. Department of Energy (DOE), Divisions of Chemical and Material Sciences, under the Contract No. DE-AC02-98CH10886. O.T. acknowledges WCU (R-31-2008-000-10035-0, Korea), Berzelii EXSELENT and 3DEM-NATUR (Sweden) for financial support. K.K. was supported by Basic Science Research Program through the NRF funded by the Ministry of Education (NRF-2013R1A1A2010795). Z. Lee was supported by Mid-career Researcher Program through the NRF funded by the Ministry of Science, ICT & Future Planning (NRF-2011-0029412). J.Y.C. and Y.J.S. were supported by the National Junior Research Fellowship (NRF-2013H1A8A1003741) and the Global Ph.D. Fellowship (NRF-2013H1A2A1032644), respectively. The EXAFS experiments performed at Pohang Light Source (PLS) were supported in part by the Ministry of Education and POSTECH. We thank the National Energy Research Scientific Computing Center (NERSC) and KAUST Supercomputing Laboratory (KSL) for computational time, and Prof. S. J. Hwang (Ewha Womans Univ.) and Prof. M. Choi (KAIST) for their help in EXAFS experiments.

Author contributions

S.H.J., R.R.A., G.-G.P. and J.Y.C. conceived the idea and designed the experiments. J.Y.C., T.K., Y.J.S. and J.K. performed the experiments. Y.C. carried out DFT calculations. H.Y.J., Z.L. and O.T. performed TEM analysis. M.G.K. contributed to the EXAFS experiments and analysis. T.H.Y. and K.K. commented on the manuscript. J.Y.C., Y.C., H.Y.J., M.G.K., G.-G.P., R.R.A. and S.H.J. wrote the manuscript.

Additional information

Supplementary information accompanies this paper at <http://www.nature.com/scientificreports>

Competing financial interests: The authors declare no competing financial interests.

How to cite this article: Cheon, J.Y. *et al.* Ordered mesoporous porphyrinic carbons with very high electrocatalytic activity for the oxygen reduction reaction. *Sci. Rep.* **3**, 2715; DOI:10.1038/srep02715 (2013).



This work is licensed under a Creative Commons Attribution-NonCommercial-NoDerivs 3.0 Unported license. To view a copy of this license, visit <http://creativecommons.org/licenses/by-nc-nd/3.0>